J. Fluid Mech. (2005), *vol.* 530, *pp.* 213–222.
doi:10.1017/S0022112005003721 Printed in the United Kingdom

Oscillations of shear flow along a slotted plate: small- and large-scale structures

By A. C. SEVER AND D. ROCKWELL

Department of Mechanical Engineering and Mechanics, Lehigh University, 356 Packard Laboratory, 19 Memorial Drive West, Bethlehem, PA 18015-3085, USA
dor0@lehigh.edu

(Received 8 September 2004 and in revised form 18 January 2005)

Shear flow along a slotted plate can give rise to highly coherent, small-scale oscillations within each slot; the dimensionless frequency is an order of magnitude lower than the frequency of the classical Kelvin–Helmholtz instability. Within a given slot, the unsteady development of a swirl pattern, as well as the flow into and out of the slot, is compatible with the evolution of a large-scale structure, which shows increased agglomeration of vorticity along the surface of the plate. Moreover, the streamwise phase shift of the unsteady flow rates through the slots is in accord with the phase shift of the velocity fluctuation of the downstream propagating disturbance along either side of the plate. This phase shift is associated with development of the large-scale structure, and corresponds to a dimensionless frequency that scales on the plate length, as verified by experiments over ranges of length and inflow velocity. The value of this dimensionless frequency is close to that in the absence of the slotted plate i.e. the Kelvin–Helmholtz instability of the free shear layer.

1. Introduction

1.1. *Previous related investigations*

Self-excited oscillation of shear flow along the opening of a single cavity, as well as along an individual perforation or slot in a plate, has received considerable attention in recent decades. These classes of investigations are briefly summarized in the following.

Oscillations due to flow past a cavity in the absence of a perforated or slotted plate. Self-sustained oscillation of flow past a cavity, in the absence of a perforated or slotted plate along its opening, has been investigated extensively, as addressed in the works of DeMetz & Farabee (1977), Knisely & Rockwell (1982), Blake (1986), Gharib & Roshko (1987), Burroughs & Stinebring (1994), Howe (1997, 1998), Rockwell (1998), Ziada (1999), Zoccola & Farabee (2001), Kuo & Huang (2001), and Rowley, Colonius & Basu (2002). Active control of these oscillations has been undertaken by Ziada (1999), and Cattafesta *et al.* (2003).

Acoustically coupled oscillations due to flow past a perforated plate. Flow past a plate with a large number of holes can give rise to highly coherent oscillations, which scale on the hole diameter, if coupling occurs with an acoustic resonant mode of either the main duct or a cavity on the backside of the plate. These resonant-coupled instabilities have received considerable attention. Recent advances and overviews are described by Howe (1998), Kirby & Cummings (1998), Dickey, Selamet & Ciray (2001), and Jing *et al.* (2001).

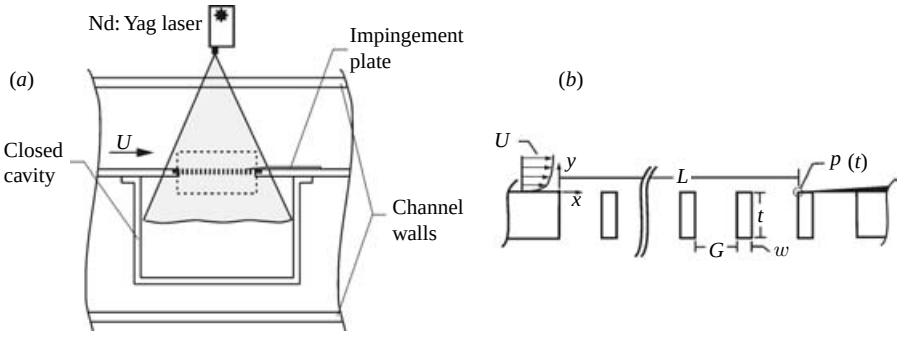

FIGURE 1. (*a*) Overview of test section showing field of view for imaging (dashed lines), and (*b*) zoomed-in view of slotted plate.

Acoustically coupled oscillations due to flow past louvres. Acoustically coupled oscillation of shear flow past louvres, or slats, located along a cavity opening, can exhibit features analogous to the acoustically coupled resonances arising from flow past perforated plates described in the foregoing, including the fact that the dominant instability scales on the gap width between louvres. These features are addressed by Bruggeman *et al.* (1991) and Looijmans & Bruggeman (1997).

Purely hydrodynamic oscillations past perforated and slotted plates. The foregoing classes of instabilities scale on the diameter of the perforation, or the gap distance between louvres, and nearly all involve coupling with an acoustic resonant mode of either a cavity on the backside of the plate or the test section. A different class of oscillations has a wavelength much larger than the perforation diameter, as described by Celik & Rockwell (2002, 2004) and Ozalp, Pinarbasi & Rockwell (2003). Furthermore, these oscillations are purely hydrodynamic, in that they are not associated with coupling with an acoustic resonant mode. Ekmekci & Rockwell (2003) have demonstrated that, in the presence of a simulated acoustic resonant mode of the bounding cavity, such coupling can occur. Zoccola (2002, 2004) has clearly shown that acoustically coupled oscillations can arise from flow past the gaps created by two-dimensional (spanwise) obstacles and slats across the opening of a cavity.

1.2. *Unresolved issues*

For the case of shear flow along a slotted (or perforated) plate, in the absence of acoustic resonant or elastic boundary effects, the following issues are unresolved: (i) the interaction between the development of large-scale structures along the surface of the plate and small-scale structures within the slots; (ii) the relationship between the downstream propagating wave system on either side of the slotted plate and the magnitude and phase shift of the unsteady volume flux through successive, individual slots; (iii) the form and degree of vorticity agglomeration of the developing large-scale structure along either side of the slotted plate; and (iv) the flow structure at the trailing edge of the plate, which can serve as a source-like region of upstream influence. The present investigation aims to clarify these features.

2. Experimental system and techniques

A test section insert was placed within the main test section of a large-scale water channel having a length of 5485 mm, a width of 610 mm and a depth of 610 mm. This insert includes a slotted plate–cavity system, which is shown in figure 1. The cavity

was sufficiently large to preclude localized recirculation zones at the leading and trailing edges of the backside of the plate. At the relatively low velocities employed herein, the cavity and the slotted plate are rigid. That is, elasticity effects are not an issue. In addition, the acoustic wavelength is two orders of magnitude larger than the characteristic length of the cavity, so acoustic resonant effects are not present. In the absence of such acoustic resonance within the cavity, its length and depth do not influence the physics of the oscillation described herein. In essence, the bounding cavity imposes a mass conservation constraint on the instantaneous inflow and outflow through the slots of the perforated plate.

The effective length L of the slotted plate could be varied via a sharp edge that translated along its surface. For the present experiments, $L = 122.5$ mm. Additional experiments, not included herein, involved variation of L over the range $79.2 \leqslant L \leqslant 152.4$ mm. The frequency f of the coherent oscillation varied such that the scaling relation $fL/U \approx 0.5$ was satisfied. In addition, experiments were also performed by variation of the inflow velocity U over the range $160 \leqslant U \leqslant 570\,\mathrm{mm\,s^{-1}}$. Again, the variations of frequency f were such that the scaling relation is $fL/U \approx 0.5$. This class of unstable oscillation is therefore robust over a range of L and U. The present report focuses on the detailed physics of the generic oscillation.

According to the definitions of figure 1, the slotted plate had values of thickness $t = 6.4$ mm, width $w = 1.9$ mm, and gap $G = 8.5$ mm, corresponding to an open area ratio of 83%. The height h of the slotted plate was $h = 76.2$ mm. The free-stream velocity was $U = 41.0\,\mathrm{cm\,s^{-1}}$. The inflow boundary layer at the leading edge of the slotted plate was turbulent and had a momentum thickness $\theta = 2.0$ mm.

High-image-density particle image velocimetry was employed to determine simultaneously the flow patterns on either side of the slotted plate, as well as within the slots. The plate was made of optically transparent Plexiglas, which allowed transmission of laser light with adequate intensity to allow sharply defined images in regions within and surrounding each of the slats. The flow was seeded with 12 micron, neutrally buoyant particles. These particles were illuminated with a laser sheet having a thickness of 1 mm, as depicted in figure 1. This sheet was generated with the aid of a cylindrical-spherical lens arrangement attached to the output of a double-pulsed, dual Nd:Yag laser combination; each laser had a power rating of 90 mJ. Patterns of particle images were recorded on a CCD camera with an array of 1024×1024 pixels at a rate of $30\,\mathrm{frames\,s^{-1}}$. Cross-correlation of particle image patterns was performed with interrogation window sizes of 32×32 pixels for preliminary interrogation, and 16×16 pixels for final evaluation. These windows were overlapped by 50%, in order to satisfy the Nyquist criterion. Each image contained a total of 7200 velocity vectors. Since the effective framing rate of the camera was fifteen frames per second and the characteristic frequency of the unsteady events was of the order of one cycle per second, the temporal evolution of the flow was well resolved, thereby allowing global evaluation of spectra and cross-spectra.

3. Evolution of large-scale structure along plate relative to small-scale structures within slots

Figure 2 shows patterns of phase-averaged velocity $\langle \boldsymbol{V} \rangle_p$ over a time span corresponding to approximately one complete oscillation cycle. The frequency (or period) of oscillation was determined from the elapsed time for repetition of a given flow event in the cinema sequence; as a complement, spectral analysis of the pressure fluctuation of the trailing edge of the plate was employed. Since the oscillation was

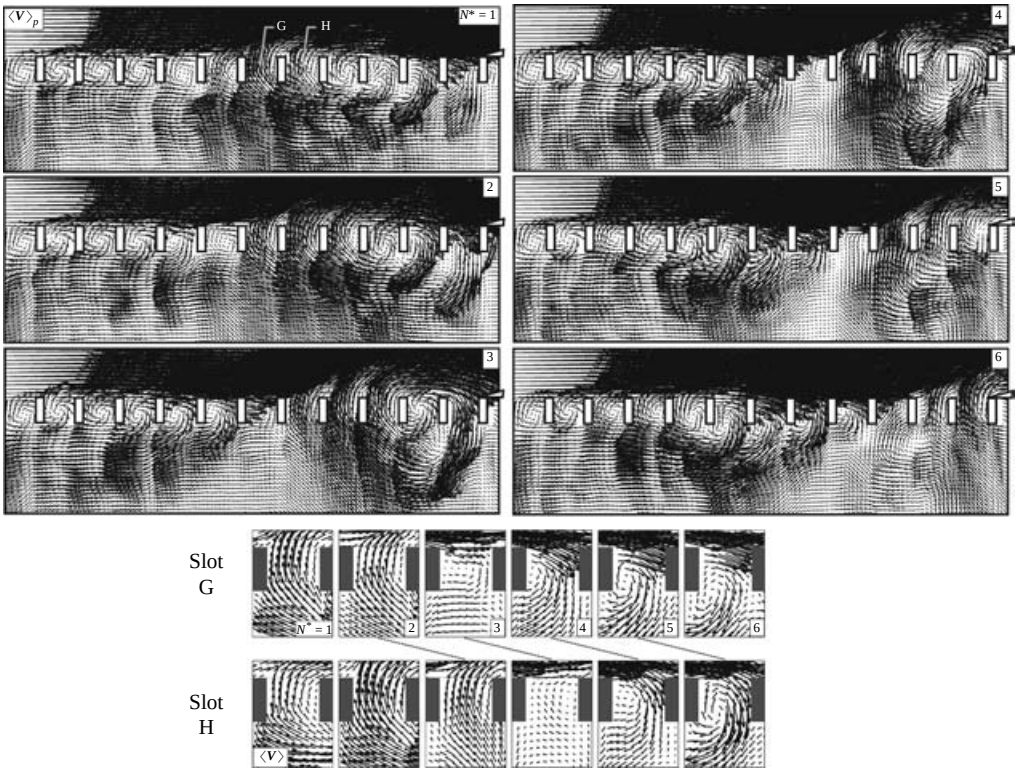

FIGURE 2. Phase-averaged patterns of velocity vectors $\langle \boldsymbol{V} \rangle_p$, which show development of flow structure with image number N^* of cinema sequence. Bottom two rows of images show development of patterns in gaps G and H.

highly coherent and repetitive, image-based phase referencing could be employed. It involved occurrence of flow structures at defined locations during the oscillation cycle; a key event was the onset of maximum jet velocity through the last slot of the plate.

The frame numbers $N^* = 1$ to 6 represent excerpts from the cinema imaging described in the previous section. Consider, first of all, the large-scale swirl pattern evident at $N^* = 1$ over the right half of the slotted plate. With increasing time, $N^* = 1$, 2 and 3, this swirl pattern becomes more compact and at a still later time, $N^* = 4$, it loses its organized structure as it interacts with the trailing end of the plate. Its successor is first evident in the left half of the image at $N^* = 3$, but not until $N^* = 6$ does this nascent swirl pattern show a clearly ordered form.

The development of these large-scale patterns is associated with well-defined, small-scale patterns within and beneath each slot. Zoomed-in images of representative slots are shown at the bottom of figure 2. They correspond to slots G and H defined in the first image at the top of figure 2. The lines connecting the sets of G and H images indicate that a given pattern in slot H is phase-shifted, i.e. delayed, with respect to the pattern in slot G, thereby indicating that the unsteadiness in the slots is moving in the downstream direction. Consider the sequence of patterns in slot G. At $N^* = 1$ and 2, flow is ejected upward through the slot. At $N^* = 3$, the flow pattern is abruptly altered; along the upper surface of the slot, downward deflection into the slot occurs, and, simultaneously, a swirl pattern is formed. At successive times $N^* = 4$,

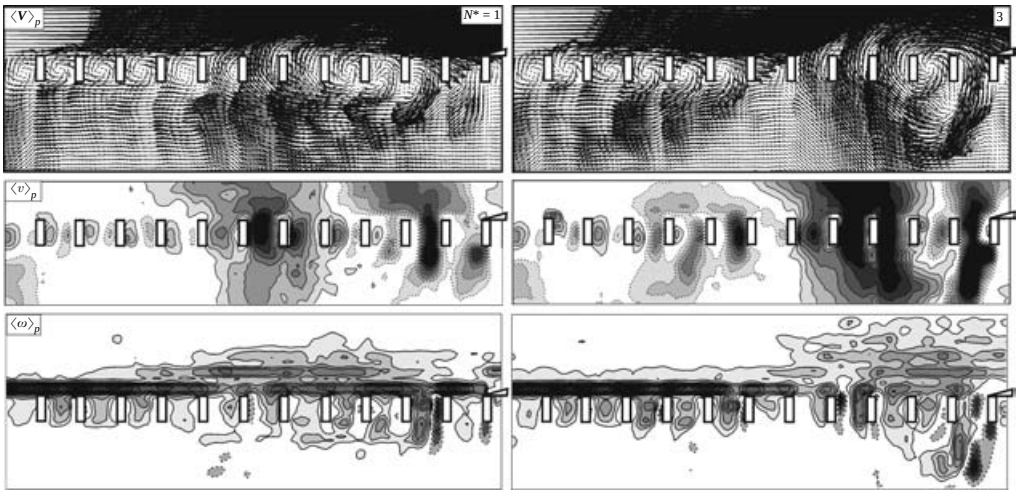

FIGURE 3. Patterns of phase-averaged velocity vectors $\langle \boldsymbol{V} \rangle_p$, vertical component $\langle v \rangle_p$ and vorticity $\langle \omega \rangle_p$ at two representative image numbers N^* in cinema sequence.

5 and 6, this downward deflection along the upper edge of the slot continues, the centre of the swirl pattern moves further downward to a location beneath the slot, and an upstream-oriented jet-like front develops. For all slots, the consequence of the localized, smaller-scale motions within and beneath each slot is the aforementioned sequence of upstream oriented fronts of velocity vectors. In fact, in patterns $N^* = 1$ to 3 of the overview images of figure 2, it appears that these fronts, which have velocity vectors of relatively large magnitude, appear to move in the upstream direction, thereby suggesting upstream disturbance propagation along the lower region of the slotted plate. This apparent upstream movement is, however, simply a manifestation of the unsteady motion through each slot, which is compatible with development of the large-scale swirl pattern, evident at $N^* = 1$, and the onset of its successor at $N^* = 2$ and 3. This aspect is further addressed below using a technique of global spectral analysis.

Figure 3 shows, in the second row of images, contours of constant phase-averaged vertical velocity $\langle v \rangle_p$, in relation to the patterns of velocity vectors $\langle \boldsymbol{V} \rangle_p$ at $N^* = 1$ and 3. Contours of downward oriented $\langle v \rangle_p$ are indicated by dashed lines, while upward-oriented $\langle v \rangle_p$ are designated by solid lines. At $N^* = 1$, regions of large magnitude $\langle v \rangle_p$ in the downward and upward directions through the indicated slots are marked by dark shading. At the later instant $N^* = 3$, the spatial extent of large magnitude $\langle v \rangle_p$, in both the downward and upward directions, becomes larger and, simultaneously, the streamwise distance between their positive and negative extrema decreases. That is, the swirl pattern becomes much more compact as it approaches the trailing edge of the plate, which was already suggested by the patterns of velocity vectors $\langle \boldsymbol{V} \rangle_p$ in images $N^* = 1$ and 3.

Patterns of phase-averaged vorticity $\langle \omega \rangle_p$ corresponding to the instants $N^* = 1$ and 3 are given in the bottom row of figure 3. The highest levels of vorticity are located above the slotted plate, as well as in individual slots, with only selected, small-scale concentrations evident beneath the plate, except in the region of the trailing edge. Consider, first of all, the large-scale cluster of $\langle \omega \rangle_p$ along the outer (upper) surface of the plate, evident at $N^* = 1$. It is approximately coincident with the large-scale pattern of velocity vectors at $N^* = 1$ in figure 2. At the later instant $N^* = 3$, this

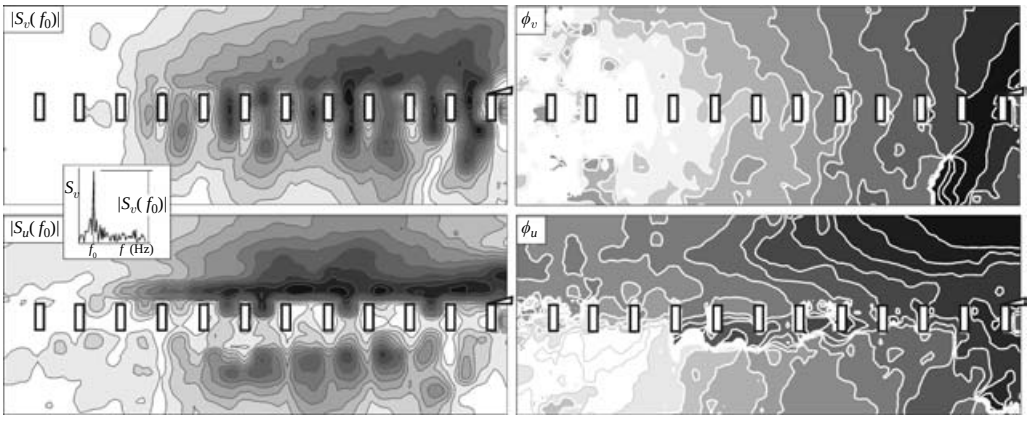

FIGURE 4. Contours of constant peak spectral amplitudes $|S_v(f_o)|$ and $|S_u(f_o)|$ and phase ϕ_v and ϕ_u of transverse v and streamline u velocity components.

relatively elongated, large-scale cluster has become much more focused into a well-defined concentration, with little change in the peak value of vorticity. Small-scale concentrations of opposite-signed vorticity occur within, or adjacent to, the slots. They are due to jet-like flows through the slots.

4. Global patterns of spectral amplitude and phase of fluctuations

Figure 4 shows the results of global spectral and cross-spectral analysis. Since the characteristic frequency of the large-scale oscillation is much lower than the effective framing rate of the imaging system, as described in § 2, it is possible to construct a well-resolved time history of the velocity fluctuation at each grid location of the flow field. This time history was evaluated for the transverse v and streamwise u velocity fluctuations at 7200 points. Then, at each location, spectra S_v and S_u were evaluated. A schematic of a representative spectrum is shown in the inset of figure 4. The pronounced peak at f_0 corresponds to the frequency of the large-scale instability, and the amplitude of this peak is indicated as $|S_v(f_0)|$. The same designation holds for the amplitude peak $|S_u(f_0)|$ of the u spectrum.

Contours of constant peak amplitude are shown in the left column of figure 4. Regarding the contours of $|S_v(f_0)|$ shown in the top left image, they have significantly large values only over the right three-fourths of the plate and maximum fluctuation levels generally occur within the slots. The spatial extent of high amplitude is largest in the last slot. Regarding the contours of $|S_u(f_0)|$, the largest values occur along the upper edge of the slotted plate. In addition, well-defined concentrations of $|S_u(f_0)|$ occur in the region beneath the plate. They tend to have a wavelength the same as the slot spacing, and are associated with the upstream-oriented, jet-like fronts along the lower side of the plate shown in figure 2.

The dimensionless frequency corresponding to the peaks of the aforementioned spectra of the transverse v and streamwise u velocity fluctuations is $f_0G/U = 0.034$, in which G is the gap width. It is important to note that this value of f_0G/U is an order of magnitude lower than the dimensionless frequency of a Kelvin–Helmholtz instability across the gap; when such an instability exists, the value of f_0G/U is of the order of 0.5, as described in the citations given in the Introduction. This observation emphasizes that the unsteady features of the zoomed-in patterns in slots G and H,

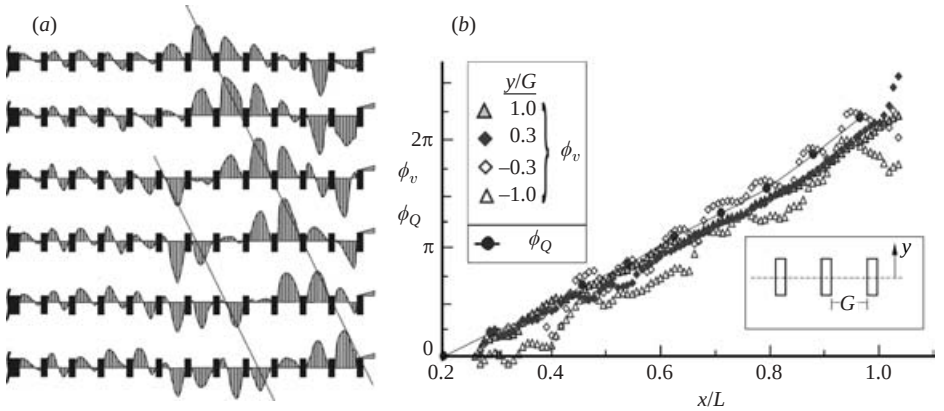

FIGURE 5. (*a*) Instantaneous distributions of vertical velocity v within slots; and (*b*) time-averaged phase ϕ_v v of vertical velocity at various horizontal elevations, as well as phase ϕ_Q of volume flux through slots.

shown at the bottom of figure 2, are not associated with an inherent hydrodynamic instability across the slot; rather they are compatible with the development of the large-scale structure along the plate. Remarkably, the dimensionless frequency of occurrence of the large-scale structure, $f_0 L/U = 0.49$, where L is the plate length, has a value that approximates the Kelvin–Helmholtz instability along the cavity opening of length L in the absence of the slotted plate, i.e. $f_0 L/U \approx 0.5$. For both of these configurations, if the phase velocity is taken as $0.5U$, the wavelength of the instability is therefore of the order of the length L.

In order to further characterize the nature of the propagating disturbance along the upper and lower sides of the slotted plate, cross-spectral analysis was performed using the same general approach as for the aforementioned spectral analysis. The reference signal was located at $x/L = 0.96$ and $y/L = 0.02$. The phase angles determined from this cross-spectral analysis are designated as ϕ_v and ϕ_u for the cross-stream (transverse) and streamwise velocity fluctuations respectively. The contours of constant phase ϕ_v shown in the image at the upper right of figure 4 indicate that identifiable lines of constant phase extend from the region above the slotted plate, through the slots, and beneath the plate, at least over the middle portion of the image. This observation indicates a rightward propagating wave system, both above and below the plate. In the region near the trailing edge, however, these phase contours are distorted in the domain beneath the plate, relative to those above the plate. This distortion is associated with the fluctuating jet flow, which has a large magnitude beneath the plate, as shown in figures 2 and 3. Regarding the contours of constant phase ϕ_u corresponding to the streamwise u component, given in the image at the lower right of figure 4, they are well defined only in the region above the plate. Below the plate, these contours show substantial jitter; nevertheless, an overall gradation of the grey level is detectable. Viewing these patterns of ϕ_u in an overall sense, the phase contours beneath the plate are shifted by approximately π relative to those above the plate.

5. Fluctuations of velocity and volume flux within slots: relation to evolution of large-scale structures

For each image in the space–time sequence, it is possible to determine the instantaneous distributions of vertical velocity within each of the slots. Figure 5 shows

the instantaneous patterns at six successive instants over the times represented by frame numbers N^* of the oscillation cycle. Within each slot, approximately seven vertical velocity components could be evaluated, and the shaded region represents a curve fit of the magnitudes of these velocities. For the first to third slots, little change of the patterns of vertical velocity with time is evident. As of the fourth slot, however, significant alterations occur, as is the case for subsequent downstream slots. The angled lines drawn through crests of these shaded representations of vertical velocity have an inclination that corresponds to the convective speed of the large-scale structure. If one focuses on, for example, the last slot at the trailing end of the plate, one sees, over the first four instants $N^* = 1$ to $N^* = 4$ a downward directed flow, at $N^* = 5$ regions of both upward and downward flow, and at $N^* = 6$ an upward directed flow.

These large variations in magnitude and direction of velocity within a given slot correspond to well-defined volume fluxes out of, and into, the region bounded by the cavity. The instantaneous volume flux Q through each slot can be calculated by integration of the velocity profile represented in figure 5 over the cross-sectional area of the slot. The phase angle ϕ_Q of the fluctuating volume flux, relative to the phase of the volume flux through the last slot, was calculated using cross-spectral analysis of the time histories of Q. Figure 5(b) compares this phase angle ϕ_Q with the phase ϕ_v of the vertical component of velocity v. The values of ϕ_v are evaluated at the designated elevations above and below the slotted plate. The streamwise variations of ϕ_v exhibit local minima and maxima, due to localized variations of phase across each slot arising from viscous effects. Generally speaking, the variations of ϕ_v with streamwise distance x/L, in which L is the overall length of the slotted plate, follow the variations of the phase ϕ_Q of the volume flux Q. As a consequence, it is possible to state that, since the frequency f is invariant, the phase speed $c = 2\pi f/[\mathrm{d}\phi/\mathrm{d}x]$ of the propagating disturbance on either side of the slotted plate is in accord with the volume fluctuations within the slots. A compatibility condition therefore exists between the downstream propagating disturbance on either side of the slotted plate and fluctuations within individual slots.

6. Concluding remarks

Turbulent inflow along a slotted plate, bounded by a non-resonant cavity, can give rise to a highly coherent instability, which is characterized by development of a large-scale structure along the plate; it has a wavelength of the order of the plate length L. The dimensionless frequency $f_0 L/U \approx 0.5$ is satisfied over ranges of L and U. The same relation holds for the oscillation in the absence of the slotted plate, which gives rise to the classical Kelvin–Helmholtz instability. This observation suggests analogous features of these two types of instabilities.

The agglomeration of vorticity associated with development of the large-scale structure, which occurs along the high-speed side of the plate, first takes an elongated form, then transforms to a well-defined concentration as it approaches the trailing edge of the plate. This development is compatible with the magnitude and phase shift of the unsteady volume flux through each successive slot of the plate, which in turn is associated with generation of small-scale vorticity concentrations within each slot. Organized velocity fluctuations occur throughout the flow domain. Spectral analysis of these fluctuations indicates that a downstream propagating wave exists along either side of, and within, the slotted plate; it is interpreted in terms of the aforementioned physical events.

The foregoing scenario is clearly more complex than the instability of the separated free shear flow in the absence of the plate, which is described in the citations given in the Introduction, and has an initial region of exponential disturbance amplification, followed by the onset and development of a concentration of vorticity. The phase speed of the downstream propagating wave is, however, approximately constant for both the free shear layer and the shear flow past the slotted plate, except for the region of distortion near the trailing edge.

Furthermore, the fluctuating velocity field is highly coherent for both of these types of instabilities, apparently due to an upstream influence, which emanates from the region of severe flow distortion in the trailing edge region. For the case of the slotted plate, this distortion involves cyclic variations of the magnitude and direction of a jet at its trailing edge.

The authors gratefully acknowledge support under ONR grant N00014-01-1-0606 monitored by Dr Ron Joslin.

REFERENCES

Blake, W. K. 1986 Mechanics of Flow-Induced Sound and Vibration: Vol. 1 – General Concepts and Elementary Sources. *Appl. Math. Mech.* **42**, 138–149.

Bruggeman, J. C., Velekoop, J. C., Van Der Knapp, F. G. P. & Keuning, P. J. 1991 Flow-excited resonance in a cavity covered by a grid: theory and experiments. *Flow Modeling, Measurement and Control*, NCA-Vol. 11/FED-Vol. 130, ASME, pp. 135–144.

Burroughs, C. B. & Stinebring, D. R. 1994 Cavity Flow Tones in Water. *J. Acoust. Soc. Am.* **95**, 1256–1263.

Cattafesta, L., Williams, D., Rowley, C. & Alvi, F. 2003 Review of active control of flow-induced cavity resonance. *AIAA Paper* 2003-3567.

Celik, E. & Rockwell, D. 2002 Shear layer oscillation along a perforated surface: a self-excited large-scale instability. *Phys. Fluids* **14**, 4444–4448.

Celik, E. & Rockwell, D. 2004 Coupled oscillations of flow along a perforated plate. *Phys. Fluids* **16**, 1714–1724.

DeMetz, F. C. & Farabee, T. M. 2004 Laminar and turbulent shear flow-induced resonances. *AIAA Paper* 77-1293.

Dickey, N. S., Selamet, A. & Ciray, M. S. 2001 An experimental study of the impedance of perforated plates with grazing flow. *J. Acoust. Soc. Am.* **110**, 2360–2370.

Ekmekci, A. & Rockwell, D. 2003 Self-sustained oscillations of the shear flow past a slatted plate coupled with cavity resonance. *J. Fluids Struct.* **167**, 1237–1245.

Gharib, M. & Roshko, A. 1987 The effect of flow oscillations on cavity drag. *J. Fluid Mech.* **117**, 501–530.

Howe, M. S. 1997 Edge, cavity and aperture tones at very low Mach numbers. *J. Fluid Mech.* **33**, 61–84.

Howe, M. S. 1998 *Acoustics of Fluid-Structure Interactions*. Cambridge University Press.

Jing, X., Sun, X., Wu, J. & Meng, K. 2001 Effect of grazing flow on the acoustic impedance of an orifice. *AIAA J.* **39**, 1478–1484.

Kirby, R. & Cummings, A. 1998 The impedance of perforated plates subjected to grazing gas flow and backed by porous media. *J. Sound Vib.* **167**, 619–636.

Knisely, C. & Rockwell, D. 1982 Self-sustained low-frequency components in an impinging shear layer. *J. Fluid Mech.* **116**, 157–186.

Kuo, C. H. & Huang, S. H. 2001 Influence of flow path modification on oscillation of cavity shear layer. *Exps. Fluids* **31**, 162–178.

Looijmans, N. H. & Bruggeman, J. C. 1997 Simple vortex models for vibration and noise caused by a flow over louvers in a cavity opening. *Proc. Fluid-Structures Intl Aeroelasticity, Flow-Induced Vibration and Noise Symposium, Vol. 1*. ASME AD, 53-1, 351–359.

Ozalp, C., Pinarbasi, A. & Rockwell, D. 2003 Self-excited oscillations of turbulent inflow along a perforated plate. *J. Fluids Struct.* **17**, 955–970.

Rockwell, D. 1998 Vortex-body interactions. *Annu. Rev. Fluid Mech.* **30**, 199–229.

Rowley, C. W., Colonius, T. & Basu, A. J. 2002 On self-sustained oscillations in two-dimensional compressible flow over rectangular cavities. *J. Fluid Mech.* **455**, 315–346.

Ziada, S. 1999 Feedback control of flow-excited cavity resonance. *ASME Pressure Vessels Piping Div Publ PVP.* **389**, 325.

Zoccola, P. J. 2002 Excitation by flow over an obstructed opening. *Tran. ASME J. Appl. Mech.* **253**(2), 899–906.

Zoccola, P. J. 2004 Effect of opening obstructions on the flow-excited response of a Helmholtz resonator. *J. Fluids Struct.* **19**, 1005–1025.

Zoccola, P. J. & Farabee, T. M. 2001 On the frequency of shear tones. *Acoust. Res. Lett. Online.* **2**(1), 13–18.